Emerging Attractor in Wavy Poiseuille Flows Triggers Sorting of Biological Cells

Matthias Laumann,[1,2] Winfried Schmidt,[1] Alexander Farutin,[2] Diego Kienle,[1] Stephan Förster,[3] Chaouqi Misbah,[2,1] and Walter Zimmermann[1,*]

[1]*Theoretische Physik I, Universität Bayreuth, 95440 Bayreuth, Germany*
[2]*Universite Grenoble Alpes/CNRS UMR 5588, LIPhy, 38041 Grenoble, France*
[3]*JNCS-1/ICS-1, Forschungszentrum Jülich, 52428 Jülich, Germany*

(Received 28 November 2018; published 26 March 2019)

Microflows constitute an important instrument to control particle dynamics. A prominent example is the sorting of biological cells, which relies on the ability of deformable cells to move transversely to flow lines. A classic result is that soft microparticles migrate in flows through straight microchannels to an attractor at their center. Here, we show that flows through wavy channels fundamentally change the overall picture. They lead to the emergence of a second, coexisting attractor for soft particles. Its emergence and off-center location depends on the boundary modulation and the particle properties. The related cross-stream migration of soft particles is explained by analytical considerations, Stokesian dynamics simulations in unbounded flows, and Lattice-Boltzmann simulations in bounded flows. The novel off-center attractor can be used, for instance, in diagnostics, for separating cells of different size and elasticity, which is often an indicator of their health status.

DOI: 10.1103/PhysRevLett.122.128002

Microfluidics attracts great attention across several disciplines [1–9]. The field includes important physics-based strategies to understand the dynamics of particles in microflows and the mechanics of (deformable) cells with a great variety of applications in life science and technology. For example, studies of soft particles in suspension and their cross-streamline migration (CSM) in low Reynolds-number linear shear and Poiseuille flows provide important insights about blood flow, cell dynamics, DNA sorting, and polymer processing, among others [8–13]. Furthermore, a surprising splitting of streams of wormlike colloids in shear-thinning fluids through modulated channels was found [14]. In modulated channels with secondary flows [15] or in serpentine [16] or curved channels [17,18], for instance, particle dynamics and separation may also be driven by inertia. Very little is known about the behavior of soft microparticles such as (red blood) cells in pressure driven Newtonian fluid flows at low Reynolds number through microchannels with modulated walls. For this case, we describe the emergence of a novel second attractor for soft particles. This may give rise to promising applications in particle separation, such as biological cells with differing elasticity or size.

Segré and Silberberg reported in 1961 on CSM of rigid particles in low Reynolds-number flows through pipes [19]. Such finite Reynolds-number effects are exploited in inertial microfluidics [17,20]. When particles and channels approach the micrometer scale, it is also possible that fluid inertia does not matter and particles follow the Stokesian dynamics. In this limit, there is no CSM of rigid particles but of soft particles which are deformed by the local shear rate. This drives, for instance, tank-treading vesicles away from walls in Poiseuille and linear shear flows [9,21–25]. Away from walls the spatially varying shear rate in bulk Poiseuille flows breaks the fore-aft symmetry of the

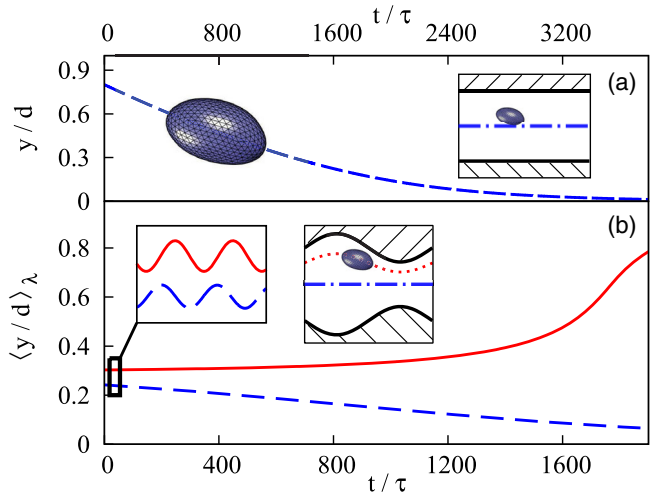

FIG. 1. (a) The trajectory of a soft capsule (dashed line) in plane Poiseuille flow approaches the attractor at the channel center at $y = 0$: The inset shows the channel cross section with the particle attractor (dash-dotted line). (b) A soft capsule in a wavy channel moves to either the off-center attractor (solid line) or to the center, depending on its initial position. The left inset shows the particle's wavy motion around the trajectory's mean (cf. animations in the Supplemental Material [38]). The right inset shows the wavy off-center particle attractor (dotted line) and the attractor at the channel center (dash-dotted line). For parameters, see [39].

 © 2019 American Physical Society

deformed particle, so that dumbbells [26,27], droplets [28,29], vesicles, and capsules [30–32] exhibit bulk CSM, even in unbounded Poiseuille flows where the interaction with the channel boundaries is neglected. Such parity breaking mechanisms may be induced spontaneously by viscosity contrast [33] or chirality [34], which are not considered here. Surprisingly, CSM of soft particles can be also reversed by gravitational effects [35]. Recently, migration was also found for nonsymmetric soft particles in time-periodic linear shear flows [36] and even in time-periodic homogeneous plug flows when particle inertia is considered [37].

As we show, soft particles in flows through wavy channels experience a periodically altering local shear rate; therefore they are periodically deformed. However, they adopt a different shape during each half period of a wavy flow. This nonsymmetric deformation causes an off-center attractor for soft particles in Newtonian fluid flow that coexists with the particle attractor at the channel center, as indicated in Fig. 1 (cf. animations in the Supplemental Material [38]).

We consider red blood cells (RBCs) and soft capsules in flows through a channel with modulated walls at

$$y_b = \pm d[1 + \varepsilon \sin(Kx)] \quad \text{with} \quad K = \frac{2\pi}{\lambda}, \tag{1}$$

with the mean boundary distance $2d$, the modulation amplitude ε, and the wavelength λ. The resulting wavy flow field $\mathbf{u}(\mathbf{r}) = (u_x, u_y, 0)$ is determined up to first order in the modulation amplitude ε (see Supplemental Material [38]) [40]

$$u_x = \tilde{u}\left(1 - \frac{y^2}{d^2} + 2\varepsilon \sin(Kx) \times [B_1 Ky \sinh(Ky) + (B_1 + B_2)\cosh(Ky)]\right), \tag{2a}$$

$$u_y = -2\tilde{u}\varepsilon \cos(Kx)[B_1 Ky \cosh(Ky) + B_2 \sinh(Ky)], \tag{2b}$$

with the flow amplitude $\tilde{u}$. The soft particle's surface is represented by N beads with radius a and located at $\mathbf{r}_i$. Their Stokesian dynamics [41] is described by a set of equations

$$\dot{\mathbf{r}}_i = \mathbf{u}(\mathbf{r}_i) + \sum_{j=1}^{N} \mathbf{H}_{ij} \cdot \mathbf{F}_j. \tag{3}$$

The particle center is at $\mathbf{r}_c = \sum_{i=1}^{N} \mathbf{r}_i / N$ and particle-wall interactions are neglected. The force on the jth bead is given by $\mathbf{F}_j = -\nabla_j V(\mathbf{r})$ with the total potential $V(\mathbf{r})$, and $\mathbf{H}_{ij}$ denoting the mobility matrix (see the Supplemental Material [38]) [42–44].

For the capsule, the total potential is $V(\mathbf{r}) = V_{\mathrm{NH}} + V_b + V_v$ with the neo-Hookean part V_{NH}, that describes rubberlike materials with a constant surface shear-elastic modulus G [45,46]. The beads form triangles as indicated in the Supplemental Material [38]. With the angles $\beta_{i,j}$ enclosed by the normal vectors at neighboring triangles and the bending elasticity κ, the bending potential is $V_b = \kappa/2 \sum_{i,j}(1 - \cos\beta_{i,j})$ [47]. The potential $V_v = k_v[\mathcal{V}(t) - \mathcal{V}_0]^2/\mathcal{V}_0$ keeps the capsules volume $\mathcal{V}(t)$ close to the reference volume $\mathcal{V}_0 = 4/3\pi R^3$ of a spherical capsule of radius R with volume stiffness k_v [48].

For the RBC we use as total potential $V(\mathbf{r}) = V_{\mathrm{Sk}} + V_{b,R} + V_v + V_a$ [48]. V_{Sk} denotes the potential of the Skalak law which describes the elastic forces of a RBC with the shear and area resistance κ_s and κ_α (see [48,49]). The bending potential is given by $V_{b,R} = \sqrt{3}\kappa_R/2 \sum_{i,j}(\beta_{i,j} - \beta_{i,j}^{(0)})^2$ where $\beta_{i,j}^{(0)}$ denotes the angles of the equilibrium shape, whereby we use the typical biconcave shape (see the Supplemental Material [38] and Ref. [50]). The potentials $V_v = k_v/\mathcal{V}_0[\mathcal{V}(t) - \mathcal{V}_0]^2$ and $V_a = k_a/\mathcal{A}_0[\mathcal{A}(t) - \mathcal{A}_0]^2$ keep deviations of $\mathcal{V}(t)$ and $\mathcal{A}(t)$ from the reference values $\mathcal{V}_0$ and $\mathcal{A}_0$ small [48]. The (dimensionless) parameters are given in Ref. [39].

We use also simulations for the particle dynamics with a standard lattice Boltzmann method (LBM) with the Bhatnager-Gross-Krook collision and the immersed boundary method [51–55]. Hereby, the effects of the channel boundary on the particle dynamics are fully taken into account.

The migration velocity $\mathbf{v}_m$ of a particle is the difference between the particle velocity $\dot{\mathbf{r}}_c$ and the undistorted flow velocity $\mathbf{u}(\mathbf{r}_c)$ at the particle's position $\mathbf{r}_c$, leading to

$$\mathbf{v}_m = \dot{\mathbf{r}}_c - \mathbf{u}(\mathbf{r}_c) = \underbrace{\sum_i \frac{\mathbf{u}(\mathbf{r}_i)}{N} - \mathbf{u}(\mathbf{r}_c)}_{=\mathbf{v}_m^f} + \underbrace{\frac{1}{N}\sum_{i,j} \mathbf{H}_{ij} \cdot \mathbf{F}_j}_{=\mathbf{v}_m^{\mathrm{HI}}}.$$

The contribution $\mathbf{v}_m^f$ is the difference between the undisturbed flow, averaged over the particle's surface, and the undisturbed flow at its center. In Poiseuille flow, the shear gradient varies across an extended particle and accordingly the particle does not follow a single streamline. The second contribution $\mathbf{v}_m^{\mathrm{HI}}$ describes the flow disturbance due to a particle.

In plane Poiseuille flow, $\mathbf{v}_m^f$ is antiparallel to the straight flow direction and causes a lag behind of particles with respect to the undistorted, local flow, but does not contribute to CSM. The classical CSM to the channel center is induced by $\mathbf{v}_m^{\mathrm{HI}}$. In a wavy channel, $\mathbf{v}_m^f$ contributes also to the migration perpendicular to the channel axis. In the diverging parts of the channel, a particle lags behind the outward directed streamline. Accordingly, the particle migrates towards a streamline closer to the center. In the

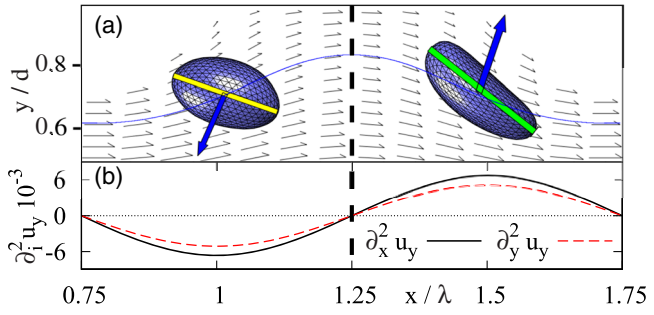

FIG. 2. (a) Two snapshots of a capsule are shown, resulting from their Stokesian dynamics simulation in an unbounded wavy flow field (black arrows). The flow is symmetric to the dashed vertical line, but the deformed particle is not (see, e.g., colored bars). (b) shows the second derivatives $\partial_x^2 u_y(x)$ and $\partial_y^2 u_y(x)$ of the vertical flow velocity u_y at $y = 0.7d$.

converging flow section the opposite is the case: The particle migrates to a streamline farther away from the center. For a rigid spherical particle in a periodically alternating diverging and converging flow at low Reynolds number, the migration steps inside and outside compensate each other and there is no net migration. However, the situation with deformable particles is different: The particle's shape is nonreciprocal during the periodically alternating converging and the diverging channel sections as indicated by the two snapshots for a capsule from Stokesian dynamics simulations in Fig. 2. This leads altogether to a net contribution of $\mathbf{v}_m^f$ to the migration away from the channel axis.

We demonstrate by a simple analytical consideration that the outward directed net migration caused by $\mathbf{v}_m^f$ may become larger than the classical inward migration driven by $\mathbf{v}_m^{\mathrm{HI}}$. By a Taylor expansion of $\mathbf{u}(\mathbf{r})$ around $\mathbf{r}_c$ and with the relations

$$\sum_i (\mathbf{r}_i - \mathbf{r}_c) = 0, \qquad \sum_i \underbrace{(x_i - x_c)(y_i - y_c)}_{\text{changes sign}} \ll \sum_i \underbrace{(x_i - x_c)^2}_{>0}$$

we obtain for the y component of $\mathbf{v}_m^f$

$$v_{m,y}^f = \frac{1}{N}\sum_i [\mathbf{u}(\mathbf{r}_i) - \mathbf{u}(\mathbf{r}_c)] \cdot \mathbf{e}_y \approx \frac{\partial_x^2 u_y}{2N}\sum_i (x_i - x_c)^2 + \frac{\partial_y^2 u_y}{2N}\sum_i (y_i - y_c)^2. \quad (4)$$

The signs of the curvatures $\partial_x^2 u_y$ and $\partial_y^2 u_y$ of the wavy flow determine the local direction of the migration velocity $v_{m,y}^f$. Their values for the imposed flow evaluated at $y/d = 0.7$ are shown in Fig. 2(b). The two sums in Eq. (4) are shape factors. They indicate that the local migration velocity increases with the deformation. In a widening channel section the signs of both curvatures are negative and therefore the migration direction points to the flow center ($v_{m,y}^f < 0$).

In the following section, the flow is converging and the signs of the curvatures are positive; i.e., the direction of $v_{m,y}^f$ points in this section away from the flow center. During the converging half period, the soft particle is stretched in flow direction with a maximum of the shape factors of about ($\sum_i (x_i - x_c)^2 = 22.8$ and $\sum_i (y_i - y_c)^2 = 17.7$). Both factors are larger than their maxima during the diverging flow part, ($\sum_i (x_i - x_c)^2 = 21.4$ and $\sum_i (y_i - y_c)^2 = 11.2$), where the capsule is compressed in the flow direction. Both shapes in Fig. 2(a) are not mirror symmetric to the dashed vertical line. Therefore, the migration velocity averaged over one spatial period, $\langle v_{m,y}^f \rangle_\lambda$, points for these parameters away from the channel center.

The curvature of the flow lines vanishes at the channel center. The local migration velocity $v_{m,y}^f$ increases at every x position with the distance from the channel center and with the boundary-modulation amplitude ε. Above a critical boundary-modulation amplitude ε_c the contribution $v_{m,y}^f$ may outweigh the classical inward migration described by $v_{m,y}^{\mathrm{HI}}$. In this case the resulting off-center attractor coexists with the attractor at the channel center at $y = 0$. Depending on the initial value of y, particles migrate either to the center or to the off-center attractor.

The trends of cross-stream migration illustrated by analytical considerations are characterized by Stokesian dynamics simulations of models for capsules and red blood cells in unbounded wavy flows and by simulations using the LBM in bounded flows. In Fig. 3, the averaged CSM velocity $\langle v_{m,y} \rangle_\lambda$ of capsules and RBCs is shown as a function of λ/R and in units of $\tilde{u}$ for two values $\tilde{u} = 5, 11$. This averaged CSM velocity is obtained by a linear fit (over a sufficient number of periods) of the lateral particle position $y(t)$, whereby the mean values of each period are used. For an initial particle position of $y = d/2$ in Fig. 3, the averaged migration direction $\langle v_{m,y} \rangle$ points to the channel center in the range of small and large values of λ/R. This means capsules and RBCs migrate in both ranges towards the channel center, similar as in unmodulated channel flows. Here, the averaged modulation-induced outward CSM, $\langle v_{m,y}^f \rangle_\lambda$, becomes small and cannot outweigh anymore the common inward migration $\langle v_{m,y}^{\mathrm{HI}} \rangle_\lambda$. This can be understood from Fig. 2: The flow's curvature plays a role only if the modulation wavelength is not much larger and not much shorter than the particle size, such as in the intermediate range of λ/R in Fig. 3. For the flow amplitude $\tilde{u} = 5$, capsules migrate in the range $7R \lesssim \lambda \lesssim 25R$ away from the channel center and the outward CSM velocity reaches a maximum at $\lambda \approx 12R$. For a larger flow velocity at the channel center $\tilde{u} = 11$, the respective ranges for capsules and RBCs are slightly shifted to larger values of λ/R. With increasing particle distance y from the channel center, the λ/R range of outward migration increases.

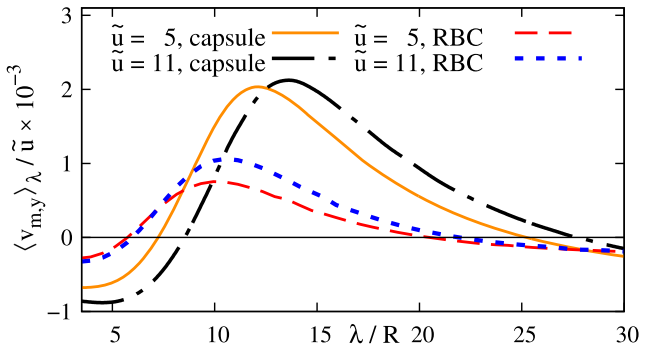

FIG. 3. The averaged CSM velocity $\langle v_{m,y}\rangle_\lambda$ of capsules and RBCs in unbounded wavy Poiseuille flow as a function of λ/R. $\langle v_{m,y}\rangle_\lambda$ is given for two amplitudes $\tilde{u} = 5, 11$. It is negative for small and rather large values of λ/R and the particles migrate to the channel center. $\langle v_{m,y}\rangle_\lambda$ is positive in the intermediate range of λ/R, where particles migrate away from the channel center. For further parameters, cf. [39].

Importantly, the qualitative behavior of the CSM velocity for capsules and RBCs is equivalent.

Figure 4 shows the averaged CSM velocity $\langle v_{m,y}\rangle_\lambda$ of a capsule in units of the flow amplitude $\tilde{u}$ and as a function of the y position of the capsule for three amplitudes $\varepsilon = 0, 0.2, 0.3$. Here, the CSM velocity results from LBM simulations of the capsule in a wavy channel, fully accounting for wall effects. In a flat channel with $\varepsilon = 0$ the capsule migrates from every $0 < y < d$ to the channel center. Beyond a critical modulation amplitude, e.g., for $\varepsilon = 0.2$, the CSM velocity is negative at $y \lesssim 0.15d$ and beyond one finds an outward migration. The zero crossing of $\langle v_{m,y}\rangle_\lambda$ at $y \approx 0.15d$ marks the position of a repeller. When a soft particle approaches the channel wall, its migration changes to the inward direction again. This means particles with $y \gtrsim 0.15d$ migrate for $\varepsilon = 0.2$ to the off-center attractor at $y \approx 0.4d$ where the migration velocity vanishes again. For a larger modulation amplitude $\varepsilon = 0.3$ the repeller is moved closer to the channel center and the attractor closer to the wall as indicated by the dashed line in Fig. 4. Hence, the results from LBM simulations for bounded Poiseuille flows confirm the analytical considerations and the results obtained by Stokesian dynamics simulations for unbounded flows.

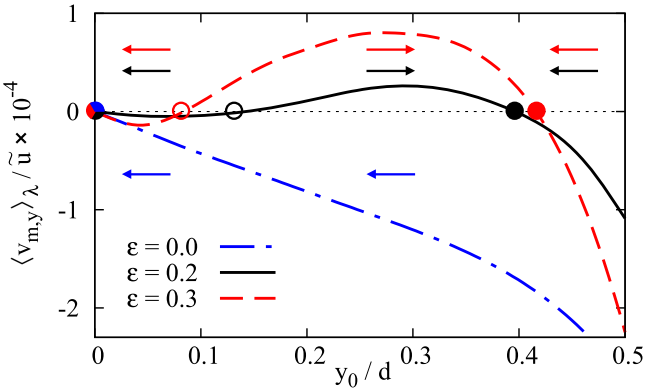

FIG. 4. The averaged migration velocity $\langle v_{m,y}\rangle_\lambda/\tilde{u}$ for capsules in bounded flows obtained by LBM simulations as a function of the particle's y position and for the modulation amplitudes $\varepsilon = 0.0,\ 0.2,\ 0.3$. The capsule migrates toward the center ($y = 0$) at small y below the repeller (empty circles) and otherwise to the second attractor (solid circles), confirming the analytical considerations and Stokesian dynamics simulations in unbounded flows. The arrows mark the migration direction, i.e., the sign of $\langle v_{m,y}\rangle_\lambda$. For further parameters, cf. [56].

Figure 5 shows the y positions of the off-center particle attractors (solid lines) and its repeller (dashed line) as a function of the boundary-modulation amplitude ε for unbounded Poiseuille flows and for three ratios $\lambda/R = 12, 16, 20$. In each case, the second attractor and the repeller appear if ε is larger than the respective critical value $\varepsilon_c = 0.14, 0.19, 0.23$. Capsules starting at a y position below the repeller migrate towards the channel center, while capsules starting above the repeller migrate to the off-center attractor. Figure 5 shows that the y positions of the second attractor and the repeller move closer to the channel center with increasing λ/R, i.e., with decreasing particle size for a given modulation wavelength λ. The off-center attractor and the repeller move also closer to the channel center with increasing stiffness of the capsules, as shown in the Supplemental Material [38].

The emergence of the second attractor for soft particles in low Reynolds-number flows through wavy channels is different to the inertia driven off-center attractors [7]. It coexists with an attractor at the channel center and this suggests a novel method for separating soft particles according to their sizes and elasticities. For instance, if two different sized particles with different radii R with $R = \lambda/20$ and $R = \lambda/12$ are injected at $y \geq 0.5d$ in a

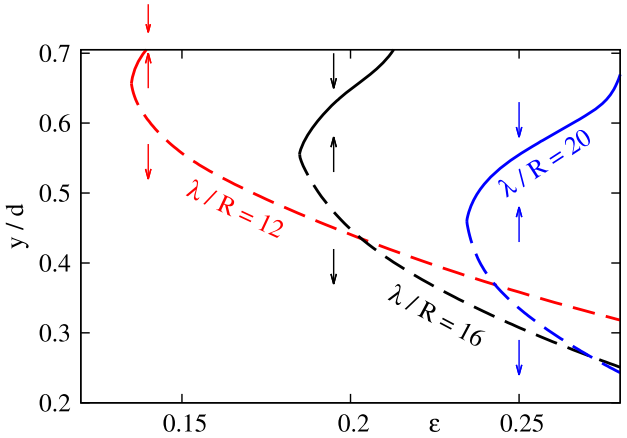

FIG. 5. The y position of the *second attractors* (solid lines) and the repellers (dashed lines) of capsules as a function of ε for $\lambda/R = 12,\ 16,\ 20$. Particles with an initial position below the repeller migrate to the channel center. The second attractor occurs for ε larger than the respective critical values $\varepsilon_c = 0.14,\ 0.19,\ 0.23$, which increase with increasing wavelength.

channel with $\varepsilon \approx 0.22$ they will be separated: The smaller particle with $R = \lambda/20$ migrates to the channel center, whereas the larger particle with $R = \lambda/12$ migrates to the off-center attractor. Hence, they can be separated with two different outlets, one at the channel center and one off center. These trends are confirmed by taking fully into account the boundary effects. For example, a capsule of radius $R = 6.6$ ($\lambda/R \approx 17$) at $y = 0.3$ migrates in LBM simulations to the wall for parameters as in Fig. 4 and a larger particle with $R = 20$ ($\lambda/R = 5.5$) to the channel center. We also remark that the migration direction does not depend on the flow direction. This allows us to utilize shorter channels simply by reversing the flow's direction in experiments.

The discovered cross-stream migration of soft particles in Newtonian fluids through wavy channels is controlled by the amplitude of the boundary modulation and the ratio of the particle size and the modulation wavelength. The origin of this CSM is the interplay between a lag behind of a particle with respect to the local flow and its asymmetric deformation in each half-period of the channel modulation. It can outweigh the classical CSM to the channel center [30–32] and induce a second, coexisting off-center attractor. This generic CSM for soft particles may play also an important role for the recently observed splitting of streams of wormlike colloids in shear thinning fluids through wavy channels [14]. Furthermore, the emergence of the second attractor allows us to separate soft particles also with respect to their stiffness (see also the Supplemental Material [38]). Since the health status of cells has been shown to affect the cell elasticity [57], our proposed approach may improve further the separation of healthy cells from malignant (e.g., cancer) cells.

For support we thank the French-German University (Grant No. CFDA-Q1-14, "Living fluids"); A. F. and C. M. the Centre National d'Etudes Spatiales; W. S. and W. Z. the Elite Study Program Biological Physics.

*Corresponding author.
walter.zimmermann@uni-bayreuth.de

[1] T. M. Squires and S. R. Quake, Rev. Mod. Phys. **77**, 977 (2005).
[2] B. J. Kirby, *Micro- and Nanoscale Fluid Mechanics* (Cambridge University Press, Cambridge, England, 2010).
[3] N.-T. Nguyen and S. T. Wereley, *Fundamentals and Applications of Microfluidics* (Artech House, Boston, 2010).
[4] A. S. Popel and P. C. Johnson, Annu. Rev. Fluid Mech. **37**, 43 (2005).
[5] E. K. Sackmann, A. L. Fulton, and D. L. Beebe, Nature (London) **507**, 181 (2014).
[6] J. B. Dahl, J.-M. G. Lin, S. J. Muller, and S. Kumar, Annu. Rev. Chem. Biomol. Eng. **6**, 293 (2015).
[7] H. Amini, W. Lee, and D. D. Carlo, Lab Chip **14**, 2739 (2014).
[8] M. D. Graham, Annu. Rev. Fluid Mech. **43**, 273 (2011).
[9] T. W. Secomb, Annu. Rev. Fluid Mech. **49**, 443 (2017).
[10] T. M. Geislinger and T. Franke, Adv. Colloid Interface Sci. **208**, 161 (2014).
[11] P. Sajeesh and A. K. Sen, Microfluid. Nanofluid. **17**, 1 (2014).
[12] C. Misbah, J. Fluid Mech. **760**, 1 (2014).
[13] A. Farutin, T. Piasecki, A. M. Slowicka, C. Misbah, E. Wajnryb, and M. L. Ekiel-Jeżewska, Soft Matter **12**, 7307 (2016).
[14] M. Schlenk, M. Drechsler, M. Karg, W. Zimmermann, R. Trebbin, and S. Förster, Lab Chip **18**, 3163 (2018).
[15] Z. Wu, Y. Chen, M. Wang, and A. J. Chung, Lab Chip **16**, 532 (2016).
[16] J. Zhang, S. Yan, R. Sluyter, W. Li, G. Alici, and N.-T. Nguyen, Sci. Rep. **4**, 4527 (2014).
[17] D. D. Carlo, Lab Chip **9**, 3038 (2009).
[18] D. D. Carlo, D. Irima, R. G. Tompkins, and M. Toner, Proc. Natl. Acad. Sci. U.S.A. **104**, 18892 (2007).
[19] G. Segré and A. Silberberg, Nature (London) **189**, 209 (1961).
[20] J. Zhang, S. Yan, D. Yuan, G. Alici, N.-T. Nguyen, M. Ebrahimi Warkiani, and W. Li, Lab Chip **16**, 10 (2016).
[21] M. S. Jhon and K. F. Freed, J. Polym. Sci., Polym. Phys. Ed. **23**, 955 (1985).
[22] I. Cantat and C. Misbah, Phys. Rev. Lett. **83**, 880 (1999).
[23] U. Seifert, Phys. Rev. Lett. **83**, 876 (1999).
[24] M. Abkarian, C. Lartigue, and A. Viallat, Phys. Rev. Lett. **88**, 068103 (2002).
[25] X. Grandchamp, G. Coupier, A. Srivastav, C. Minetti, and T. Podgorski, Phys. Rev. Lett. **110**, 108101 (2013).
[26] G. Sekhon, R. Armstrong, and M. S. Jhon, J. Polym. Sci., Polym. Phys. Ed. **20**, 947 (1982).
[27] P. O. Brunn, Int. J. Multiphase Flow **9**, 187 (1983).
[28] L. G. Leal, Annu. Rev. Fluid Mech. **12**, 435 (1980).
[29] S. Mandal, A. Bandopadhyay, and S. Chakraborty, Phys. Rev. E **92**, 023002 (2015).
[30] B. Kaoui, G. H. Ristow, I. Cantat, C. Misbah, and W. Zimmermann, Phys. Rev. E **77**, 021903 (2008).
[31] G. Coupier, B. Kaoui, T. Podgorski, and C. Misbah, Phys. Fluids **20**, 111702 (2008).
[32] S. K. Doddi and P. Bagchi, Int. J. Multiphase Flow **34**, 966 (2008).
[33] A. Farutin and C. Misbah, Phys. Rev. E **89**, 042709 (2014).
[34] N. Watari and R. G. Larson, Phys. Rev. Lett. **102**, 246001 (2009).
[35] A. Förtsch, M. Laumann, D. Kienle, and W. Zimmermann, Europhys. Lett. **119**, 64003 (2017).
[36] M. Laumann, P. Bauknecht, S. Gekle, D. Kienle, and W. Zimmermann, Europhys. Lett. **117**, 44001 (2017).
[37] I. Jo, Y. Huang, W. Zimmermann, and E. Kanso, Phys. Rev. E **94**, 063116 (2016).
[38] See Supplemental Material at http://link.aps.org/supplemental/10.1103/PhysRevLett.122.128002 for animations and for the calculation of the flow. Also details of the modeling and of the CSM of the capsule and the RBC are given.
[39] Parameters for Stokesian dynamics: (a) Flow: $u_0 = 5.0$, $d = 50$, $\lambda = 80.0$, $\varepsilon = 0.3$, $\eta = 1.0/6.0$; (b) Capsule: $G = 0.2$, $\kappa_c = 1.0$, $k_v = 1.0$, $a = 0.4$, $N = 642$, $b = 1.0$,

$R = 6.6$; (c) RBC: $\kappa_\alpha = 175.5$, $\kappa_s = 3.51$, $\kappa_R = 0.23$, $k_v = 1.0$, $k_a = 1.0$, $a = 0.2$, $N = 642$, $b = 1.0$, $R = 6.6$.

[40] S. Tsangaris and E. Leiter, J. Eng. Math. **18**, 89 (1984).

[41] J. K. G. Dhont, *An Introduction to Dynamics of Colloids* (Elsevier, Amsterdam, 1996).

[42] H. Yamakawa, J. Chem. Phys. **53**, 436 (1970).

[43] J. Rotne and S. Prager, J. Chem. Phys. **50**, 4831 (1969).

[44] E. Wajnryb, K. A. Mizerski, P. J. Zuk, and P. Szymczak, J. Fluid Mech. **731**, R3 (2013).

[45] S. Ramanujan and C. Pozrikidis, J. Fluid Mech. **361**, 117 (1998).

[46] D. Barthès-Biesel, Annu. Rev. Fluid Mech. **48**, 25 (2016).

[47] G. Gompper and D. M. Kroll, J. Phys. I (France) **6**, 1305 (1996).

[48] T. Krüger, M. Gross, D. Raabe, and F. Varnik, Soft Matter **9**, 9008 (2013).

[49] R. Skalak, A. Tozeren, R. P. Zarda, and S. Chien, Biophys. J. **13**, 245 (1973).

[50] E. Evans and Y. Fung, Microvasc. Res. **4**, 335 (1972).

[51] T. Krueger, F. Varnik, and D. Raabe, Comput. Math. Appl. **61**, 3485 (2011).

[52] P. L. Bhatnagar, E. P. Gross, and M. Krook, Phys. Rev. **94**, 511 (1954).

[53] C. K. Aidun and J. R. Clausen, Annu. Rev. Fluid Mech. **42**, 439 (2010).

[54] Z. Guo, C. Zheng, and B. Shi, Phys. Rev. E **65**, 046308 (2002).

[55] C. S. Peskin, Acta Numer. **11**, 479517 (2002).

[56] Model parameters for LBM simulations: $\lambda = 110$, channel diameter in y and z direction $d_y = 120$ (modulated walls), $d_z = 120$ (flat side walls), $\tilde{u} = 0.03$, density $\rho = 1.0$, $\eta = 1.0$; capsule: $k_v = 0.1$, $\kappa = 0.002$, $G = 0.002$, $b = 1$, $R = 6.6$, particle Reynolds number $\mathrm{Re}_\mathrm{p} = 0.4$.

[57] J. Guck, S. Schinkinger, B. Lincoln, F. Wottawah, S. Ebert, M. Romeyke, D. Lenz, H. M. Erickson, R. Ananthakrishnan, D. Mitchell, J. Käs, S. Ulvick, and C. Bilby, Biophys. J. **88**, 3689 (2005).